Journal of Zhejiang University-SCIENCE B (Biomedicine & Biotechnology)
ISSN 1673-1581 (Print); ISSN 1862-1783 (Online)
www.jzus.zju.edu.cn; www.springerlink.com
E-mail: jzus@zju.edu.cn

Novel *ACADVL* variants resulting in mitochondrial defects in long-chain acyl-CoA dehydrogenase deficiency*#

Ting CHEN[§1,2], Fan TONG[§1], Xiao-yu WU[2], Ling ZHU[1,2], Qiu-zi YI[2], Jing ZHENG[1], Ru-lai YANG[1], Zheng-yan ZHAO[1], Xiao-hui CANG[1,2], Qiang SHU[†‡1], Ping-ping JIANG[†‡1,2]

[1]*Division of Medical Genetics and Genomics, The Children's Hospital, Zhejiang University School of Medicine / National Clinical Research Center for Child Health, Hangzhou 310052, China*

[2]*Institute of Genetics and Department of Human Genetics, Zhejiang University School of Medicine, Hangzhou 310058, China*

[†]E-mail: shuqiang@zju.edu.cn; ppjiang@zju.edu.cn

Received June 22, 2020; Revision accepted Aug. 16, 2020; Crosschecked Oct. 13, 2020

Abstract: The pathogenesis of very-long-chain acyl-CoA dehydrogenase (VLCAD) deficiency is highly heterogeneous and still unclear. Additional novel variants have been recently detected in the population. The molecular and cellular effects of these previously unreported variants are still poorly understood and require further characterization. To address this problem, we have evaluated the various functions and biochemical consequences of six novel missense variants that lead to mild VLCAD deficiency. Marked deficiencies in fatty acid oxidation (FAO) and other mitochondrial defects were observed in cells carrying one of these six variants (c.541C>T, c.863T>G, c.895A>G, c.1238T>C, c.1276G>A, and c.1505T>A), including reductions in mitochondrial respiratory-chain function and adenosine triphosphate (ATP) production, and increased levels of mitochondrial reactive oxygen species (ROS). Intriguingly, higher apoptosis levels were found in cells carrying the mutant VLCAD under glucose-limited stress. Moreover, the stability of the mutant homodimer was disturbed, and major conformational changes in each mutant VLCAD structure were predicted by molecular dynamics (MD) simulation. The data presented here may provide valuable information for improving management of diagnosis and treatment of VLCAD deficiency and for a better understanding of the general molecular bases of disease variability.

Key words: Mitochondrial dysfunction; Very-long-chain acyl-CoA dehydrogenase (VLCAD); β-Oxidation; Molecular dynamics (MD) simulation
https://doi.org/10.1631/jzus.B2000339 **CLC number:** R725.8

1 Introduction

Mitochondrial fatty acid (FA) β-oxidation is a major catabolic process for degradation of long-chain FAs, the most efficient and predominant energy source for heart, liver, and skeletal muscles. Very-long-chain acyl-CoA dehydrogenase (VLCAD) controls the first step in the FA oxidation (FAO) pathway for catalysis of 14 to 20-carbon acyl-CoAs in mitochondria (Aoyama et al., 1995). VLCAD deficiency (OMIM#201475), caused by recessive mutations of acyl-CoA dehydrogenase very long chain (*ACADVL*; OMIM*609575), usually results in energy depletion

‡ Corresponding authors
§ The two authors contributed equally to this work
* Project supported by the National Natural Science Foundation of China (No. 81741090), the Zhejiang Provincial Program for the Cultivation of High-level Innovative Health Talents, and the National Key R&D Program of China (Nos. 2017YFC1001703 and 2018YFC1002700)
# Electronic supplementary materials: The online version of this article (https://doi.org/10.1631/jzus.B2000339) contains supplementary materials, which are available to authorized users
ORCID: Ting CHEN, https://orcid.org/0000-0002-0530-675X

and toxicity due to accumulation of long-chain FAs or other derivatives in the tissues (Wajner and Amaral, 2015). Although this disease is clinically heterogeneous in terms of age at onset, severity, and tissues affected, three classic phenotypes of VLCAD deficiency have been characterized: neonate onset with cardiomyopathy and hepatic failure, infant onset with liver insufficiency, or a mild adolescent-onset myopathic form. Moreover, a clear genotype–phenotype relationship is postulated between the nature of the mutation and the severity of the disease, with variants that lead to a truncated protein having the most severe presentation (Andresen et al., 1999). However, the mutations of VLCAD deficiency are diverse and broadly spread throughout the 20 exons of *ACADVL*, with few variants markedly more prevalent than others. Recently, Miller et al. (2015) found 40 novel genetic variants and 54 reported pathogenic *ACADVL* alleles in 1080 subjects. A survey of cohort of 52 individuals with VLCAD deficiency revealed another 26 novel *ACADVL* variants (Pena et al., 2016). As progress in diagnosing VLCAD deficiency continues, more variants are likely to be identified (Zhang et al., 2014; Li et al., 2015); however, the effects of several novel missense variants on residual metabolic capacities are unknown and still need to be characterized.

FAO produces acetyl-CoA to fuel the tricarboxylic acid (TCA) cycle and feeds electrons into the respiratory chain directly for generation of adenosine triphosphate (ATP). Thus, disturbance of mitochondrial energy homeostasis is considered a crucial aspect of the pathology of VLCAD deficiency (Lim et al., 2018; Seminotti et al., 2019). Additional data have also demonstrated that metabolite accumulation in VLCAD deficiency disrupts mitochondrial bioenergetics (Cecatto et al., 2018). Mitochondrial dysfunction due to VLCAD deficiency is responsible for hepatic steatosis and hepatic insulin resistance (Zhang et al., 2007). Other research has suggested that mitochondrial dysfunction due to FAO defects is associated with alterations in inflammatory processes, cellular immunity, and cell fate determination (Buck et al., 2016; Nomura et al., 2016; Xiong, 2018).

The various symptoms of VLCAD deficiency are associated with a wide variety of genetic mutations. Recent work has indicated that the function of *ACADVL* variants is likely dependent on the type and/or position of the protein domain, particularly missense variants (Miller et al., 2015; Obaid et al., 2018). However, the investigation of mitochondrial function and molecular consequences of novel missense variants in VLCAD-deficiency patients remains limited. Recently, six novel missense variants in *ACADVL* (NM_000018.3), c.541C>T (p.H181Y), c.863T>G (p.F288C), c.895A>G (p.K299E), c.1238T>C (p.I413T), c.1276G>A (p.A426T), and c.1505T>A (p.L502Q), were identified in nine neonates diagnosed through newborn screening in Zhejiang Province, China (Tong et al., 2019). In this study, we construct stable transfectants with haemagglutinin (HA)-tagged wild-type (WT) or mutant versions of VLCAD in human embryonic kidney 293T (HEK293T) cells to validate the effects of these mutants on FAO capacity and mitochondrial function, including respiratory chain function, ATP production, and creation of reactive oxygen species (ROS). In addition, we have carried out molecular and protein stability analyses, to understand the specifical effects of each variants on disease variability for improving future diagnosis and prognosis.

2 Materials and methods

2.1 Patients and novel variants

Nine unrelated patients were recruited between 2009 and 2017 via the neonatal screening program at the newborn screening center of the Children's Hospital, Zhejiang University School of Medicine, Hangzhou, China. All VLCAD-deficient patients were clinically diagnosed by detecting elevation of C14:1 FA and elevated C14:1/C8 FA ratio, followed by molecular analysis of *ACADVL* for confirmation. The variants, genotypes, and analysis of amino acid conservation of VLCAD across different species are available in Fig. S1. Most variants were found in patients with mild VLCAD-deficiency syndrome, except for c.1505T>A carried by one neonate-onset patient with a reported truncating c.1280G>A (p.W427X) together (Tong et al., 2019). All variants are numbered according to the NM_000018.3 reference sequences. Informed consent, blood samples, and clinical evaluations were obtained from all participants and families, under a protocol approved by the Ethics Committees of the Children's Hospital, Zhejiang University School of Medicine. All methods were

performed in accordance with relevant guidelines and regulations.

2.2 Vector construction and cell culture

The full-length *ACADVL* (*Homo sapiens*) sequence was amplified by polymerase chain reaction (PCR) from vector PCMV-SPORT6 (YouBio Technology Co., Ltd., Shaanxi, China), and subcloned into the *Eco*R1/*Xba*1 sites of the pRK3-HA. Besides the WT, seven plasmids with mutant *ACADVL*-HA were generated into pcDNA3.1 with Mut Express II Fast Mutagenesis Kit V2 (Vazyme Co., Ltd., Nanjing, China; C214-01), containing the six variants above and a previously reported pathogenic variant c.1153C>T (p.R385W) in family 5 as a positive control (Boneh et al., 2006). HEK293T cells were routinely cultured in Dulbecco's modified Eagle's medium (DMEM) supplemented with 10% fetal bovine serum (FBS) and 1% penicillin/streptomycin. Plasmid transfection was carried out with jetPRIME® (Polyplus-transfection® SA, France). Stable cell clones were selected by zeocin (400 μg/mL). Protein expression in transiently transfected cells or the stable clones was monitored by western blotting (Fig. S2).

2.3 Mitochondrial respiration assay

Oxygen consumption rate (OCR) of transfected cultured HEK293T cells was tested on the Seahorse Bioscience XFe96 analyzer (Agilent, Seahorse Bioscience, MA, USA) with the XF Cell Mito Stress Test Kit (Agilent Technologies, Shanghai, China) in a cell density of 20000 per well. Inhibitors were programmed injected at the following concentrations: oligomycin, 1.5 μmol/L; carbonyl cyanide 4-trifluoromethoxy-phenylhydrazone (FCCP), 0.15 μmol/L; antimycin A, 5 μmol/L; and rotenone, 1 μmol/L.

2.4 FAO of cellular respiration and FAO flow cytometry

The ability of transfected cultured HEK293T cells to oxidize exogenous FAs was measured by XF Palmitate-BSA FAO substrate on the Seahorse Bioscience XFe96 analyzer (Agilent Technologies) according to the manufacturer's protocol. Cells were cultured without glucose for 12 h before inoculating to the XF96 culture plate. One day later, 30 μL XF Palmitate-BSA FAO substrate or bovine serum albumin (BSA) was added to cells and probed with the following inhibitors: oligomycin, 1.5 μmol/L; FCCP, 0.6 μmol/L; antimycin A, 5 μmol/L; and rotenone, 1 μmol/L. The capacity of FAO was also tested by the Fatty Acid Oxidation Human Flow Cytometry Kit (Abcam, Cambridge, UK; ab118183).

2.5 ATP and mitochondrial superoxide measurements

Whole-cell and mitochondrial ATP levels were measured using the CellTiter-Glo Luminescent Cell Viability Assay Kit (Promega, WI, USA) on the Synergy H1 Hybrid Reader (BioTek, VT, USA), according to protocols described elsewhere (Jiang et al., 2016). In brief, a total of 3×10^4 cells were incubated for 2 h in the record solution (156 mmol/L NaCl, 3 mmol/L KCl, 2 mmol/L $MgSO_4$, 1.25 mmol/L KH_2PO_4, 2 mmol/L $CaCl_2$, 20 mmol/L 4-(2-hydroxyethyl)-1-piperazineethanesulfonic acid (HEPES), pH 7.35) with 10 mmol/L glucose (for total ATP measurement) or 5 mmol/L 2-deoxy-D-glucose plus 5 mmol/L pyruvate (for mitochondrial ATP measurement). Next, cells were lysed with CellTiter-Glo reagents and measured on a Synergy H1 Hybrid Reader (BioTek).

Mitochondrial superoxide was evaluated with Mito-SOX-Red (Invitrogen, CA, USA) as elsewhere (Yu et al., 2014). Briefly, 3×10^5 cells were harvested, resuspended in 5 mmol/L Mito-SOX reagent working solution, and then incubated at 37 °C for 20 min. After washing twice with phosphate-buffered saline (PBS), cells were resuspended in PBS in the absence or presence of 2 mmol/L freshly prepared H_2O_2 and 2% FBS and then incubated at room temperature for another 25 min. Samples with or without H_2O_2 were further washed with PBS and finally measured using the NovoCyte Flow Cytometer (ACEA Biosciences, CA, USA).

2.6 Western blotting

Western blotting was performed as detailed previously (Zhao et al., 2018). A total of 20 μg protein from cell lysis was analyzed by sodium dodecyl sulfate-polyarylamide gel electrophoresis (SDS-PAGE). The primary commercial antibodies were used: VLCAD (Abcam, ab155138), HA-Tag (CWBIO, Beijing, China, CW0092), β-actin (Beyotime, Shanghai, China, AF0003), and ACADM (Abcam, ab110296). Peroxidase-conjugated goat anti-mouse IgG (Beyotime, A0216) and goat anti-rabbit IgG (Beyotime, A0208) were used as secondary antibodies. Protein signals were detected using the electrochemiluminescence (ECL) system (Millipore, MA, USA).

2.7 Apoptosis assay

Apoptosis was evaluated using an APC Annexin V Apoptosis Detection Kit with PI Kit, according to the manufacturer's instructions (BioLegend, San Diego, CA, USA). Prior to the assay, cells were cultured in medium with glucose (4.5 mmol/L) or medium without glucose for 12 h. Fluorescence was determined with a NovoCyte Flow Cytometer (ACEA Biosciences).

2.8 Blue native PAGE

Blue native (BN)-PAGE was carried out using total proteins obtained from control and mutant cell lines as detailed previously (Wittig et al., 2006). Briefly, cell pellets were suspended in 2% *n*-dodecyl β-D-maltoside (DDM; Sigma-Aldrich, MO, USA; D4641-500MG) solution containing 50 mmol/L NaCl, 50 mmol/L imidazole, 2 mmol/L 6-aninohexanoic acid, and 1 mmol/L ethylene diamine tetraacetic acid (EDTA; pH 7.4) on ice for 10 min. After removing insoluble material by centrifugation, a total of 10 μg protein from each sample was loaded onto a 3%–12% (1%=0.01 g/mL) gradient Native PAGE Bis-Tris gel. Gels were run at 150 V in dark blue cathode buffer for 1 h, and then at 250 V in light blue running buffer for 1.5 h at 4 °C. The native gels were prewashed in transfer buffer (25 mmol/L Tris, 192 mmol/L glycine, 20% methanol), and then transferred to a polyvinylidene fluoride membrane for immunoblotting. The antibodies used for this experiment were HA-Tag (CWBIO, CW0092) and goat anti-mouse IgG (Beyotime, A0216).

2.9 Molecular dynamics simulation analyses

The initial coordinates of human WT VLCAD were taken from the crystal structure of VLCAD (Protein Data Bank (PDB) ID: 2UXW), whereas the coordinates of missed residues were obtained by I-TASSER (Yang et al., 2015). The structure at 33 ns was used as the template for generating the coordinates of the mutations H181Y, F288C, R385W, I413T, and A426T by PyMOL (Bramucci et al., 2012). Simulations were conducted using the GROMACS 4.5.5 package (Hess et al., 2008) with CHARMM36 force field parameters (Huang and Mackerell, 2013). The proteins were dissolved in a cubic box with 50 mmol/L NaCl in each system. Energy minimization was equilibrated with the Steepest Descent algorithm to relieve unfavorable contacts. Positional constraints were applied successively on H-bonds of heavy atoms, main-chain atoms, and Cα atoms using the LINear Constraint Solver (LINCS) algorithm (Hess, 2008). The NVT ensemble was set up to 50 ps with a time step of 1 fs from 50 to 310 K in the first step, whereas the NPT ensemble proceeded with a time step of 2 fs to equilibrate the solvent, and maintained at 310 K and 1 bar for the whole system on the rest steps (Berendsen et al., 1984). Electrostatic interactions were calculated by the particle mesh Ewald (PME) algorithm (Essmann et al., 1995). The trajectories of VLCAD were visualized with visual molecular dynamics (VMD) software (Humphrey et al., 1996).

2.10 Statistical analysis

Data were analyzed using GraphPad Prism software 8.0 and expressed as mean±standard deviation (SD) unless otherwise noted. A P value less than 0.05 was considered to be statistically significant by an unpaired, two-tailed Student's t-test.

3 Results

3.1 Influence of variants on FAO capacity

To determine whether the VLCAD variants influenced key enzymes of mitochondrial FAO, we overexpressed each of the seven recombinant HA-tagged mutant proteins in HEK293T cell lines as well as WT protein as a control, and then checked protein expression levels in each. As shown in Fig. S2, immunoblotting with anti-HA demonstrated that missense variants did reduce exogenous VLCAD expression in transiently transfected cells, compared with the control. To exclude the influence of VLCAD protein concentrations on experiments results, we selected stable transfected cell clones with similar protein levels and then compared FAO metabolism in these clones. No significant reduction was found in either the level of medium-chain specific acyl-CoA dehydrogenase (MCAD) or the level of α subunit of the hydroxyacyl-CoA dehydrogenase (HADHA) between mutant and control cell lines. However, the relative enzyme levels of mutant VLCAD were 50.9%, 33.0%, 86.3%, 19.3%, 47.9%, 36.3%, and 49.7% compared to those of the control (Fig. 1a). To further confirm whether those variants reduced the

enzyme's ability to oxidize exogenous FAs, we carried out OCR tests of FAO with exogenous palmitate supply in a glucose-limited medium. Only barely detectable FAO capacity was detected in cells carrying the variants (c.863T>G, c.895A>G, c.1153C>T, c.1238T>C, c.1276G>A, and c.1505T>A) in the presence of palmitate, while cells containing the c.541C>T variant showed a relative FAO capacity of 46.1% compared to the mean value of the control (Figs. 1b and S3). These data suggest that these variants have a lower capacity to utilize FAs when responding to stressful energy demand.

3.2 Influences of variants on mitochondrial respiratory function, ATP production, and ROS

To further evaluate whether the variants perturbed the energy homeostasis, we assessed mitochondrial respiratory function, ATP production, and mitochondrial superoxide generation among different cell lines (Fig. 2). No apparent differences in oxygen consumption were present in the control and untreated HEK293T lines. However, a marked deficiency of OCR was exhibited in most of the mutant cell lines, as can been seen from the rate of basal-OCR, ATP-linked OCR, and maximal-OCR in mutant cell lines. For instance, in each of the mutants, the rates of maximal-OCR, an indicator for the cellular capacity of flexibility responses due to stress, were 56.0%, 38.2%, 37.8%, 62.3%, 54.6%, 28.0%, and 55.3% of the mean value in the control lines. However, the c.541C>T variant was comparable to the control in basal-OCR and ATP-linked OCR. As the OCR linked to ATP production was decreased significantly, we then measured the level of whole-cell and mitochondrial ATP generation using a luciferin/luciferase assay (Fig. 2b). Reduction of both whole-cell and mitochondrial ATP was found in the mutant cell lines; in these variants, mitochondrial ATP was 82.1% (c.541C>T), 67.2% (c.863T>G), and, 59.8% (c.895A>G), 39.8% (c.1153C>T), 45.0% (c.1238T>C), 52.0% (c.1276G>A), and 58.4% (c.1505T>A), compared to that of the control. A small decrease in mitochondrial ATP was found in cells containing the c.541C>T variant. Because increases in mitochondrial ROS are typical of dysfunctional mitochondria, we evaluated mitochondrial superoxide levels in all variants, using a Mito-SOX-Red probe with or without H_2O_2 exposure (Fig. 2c). Strikingly, mitochondrial

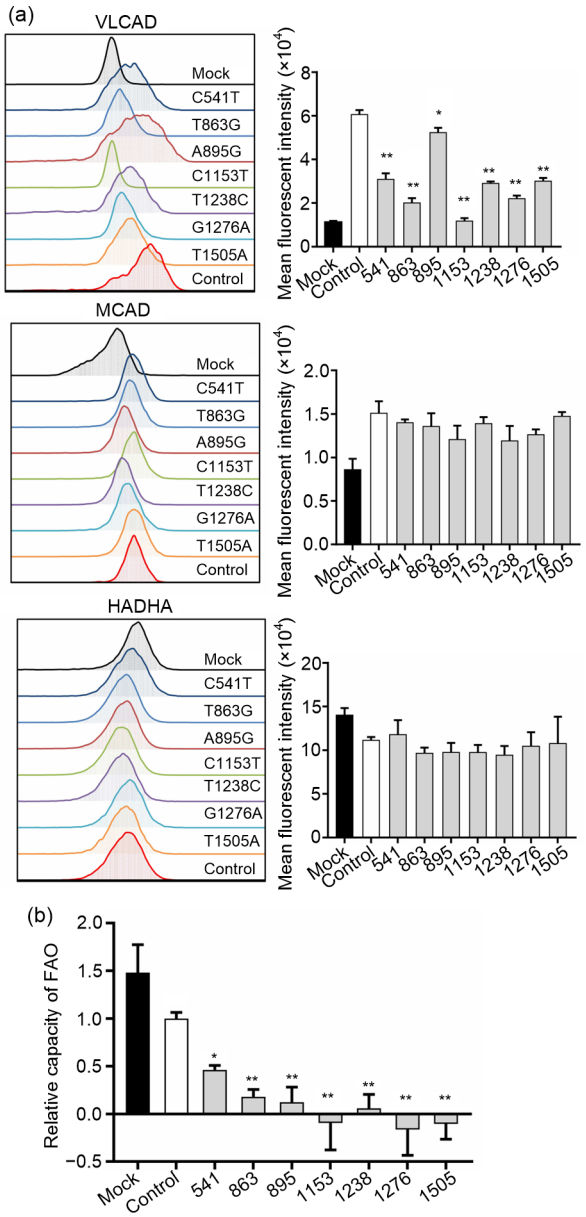

Fig. 1 FAO capacity in various cells

(a) Protein levels of three fatty acid oxidation (FAO) key enzymes assessed by flow cytometry: very-long-chain acyl-CoA dehydrogenase (VLCAD), medium-chain specific acyl-CoA dehydrogenase (MCAD), and α subunit of the hydroxyacyl-CoA dehydrogenase (HADHA). (b) Relative capacity of FAO for utilization of exogenous palmitate. The capacities of FAO in mutant cell lines were normalized to that in control. Mock, treated with vector without VLCAD; control, cells overexpressing wild-type VLCAD; 541/C541T, cell line overexpressing c.541C>T; 863/T863G, c.863T>G; 895/A895G, c.895A>G; 1153/C1153T, c.1153C>T; 1238/T1238C, c.1238T>C; 1276/G1276A, c.1276G>A; 1505/T1505A, c.1505T>A. Data were expressed as mean± standard deviation (SD) of >3 independent experiments. * $P\leq0.05$, ** $P\leq0.01$, vs. control

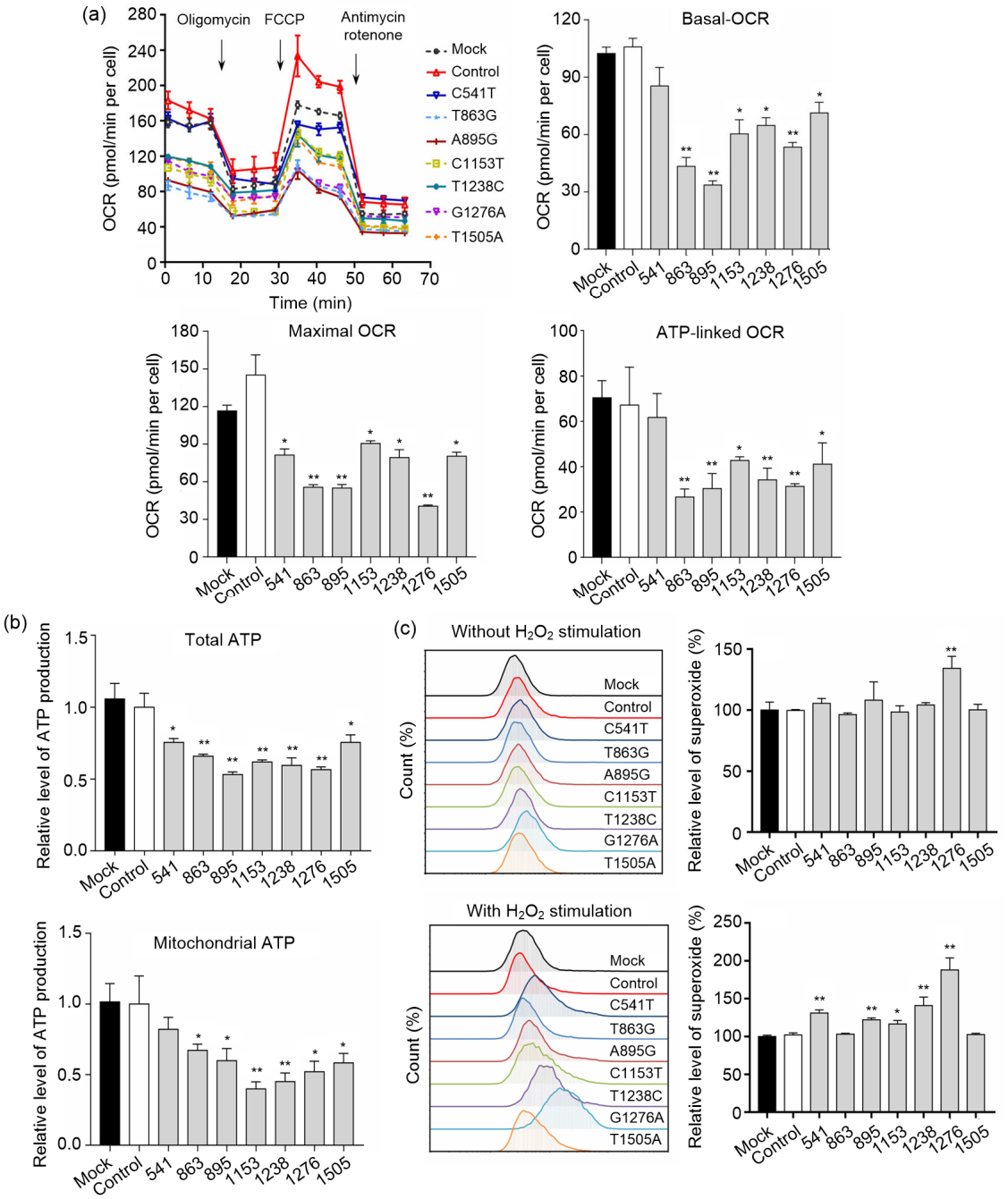

Fig. 2 Function of mitochondrial respiratory chain and alterations in superoxide production

(a) Oxygen consumption rate (OCR) assay under normal glucose conditions, including the progress curve and graphs as basal-OCR (the difference between basal-OCR and after rotenone/antimycin A treatment), adenosine triphosphate (ATP)-linked OCR (the difference between basal-OCR and the OCR following oligomycin exposure), and the maximum-OCR (the difference between OCR after carbonyl cyanide 4-trifluoromethoxy-phenylhydrazone (FCCP) uncoupling and rotenone/antimycin A treatment). (b) Measurement of whole-cell and mitochondrial ATP levels. Cells were incubated with 10 mmol/L glucose (total ATP) or 5 mmol/L 2-deoxy-D-glucose (2-DG) plus 5 mmol/L pyruvate (mitochondrial ATP) for experiments. The average ATP levels in mutant cell lines were normalized to that of the control. (c) Mitochondrial superoxide production detected by a MitoSOX-Red probe without or with H_2O_2 (1 μmol/L) stimulation. Average superoxide levels in mutant cell lines were normalized to that of the control. Data were expressed as mean±standard deviation (SD), n=5 or 6. * $P\leq0.05$, ** $P\leq0.01$, vs. control. Samples were described as in Fig. 1

superoxide levels in cells carrying c.1276G>A increased to 134.3% even without H_2O_2, and then sharply increased again to 188.0% when H_2O_2 was added. Increased levels of superoxide were also confirmed in cells carrying c.541C>T, c.895A>G, c.1153C>T, and c.1238T>C in the presence of H_2O_2, with mean levels of 131.1%, 122.2%, 116.6%, and 140.8%, respectively, relative to the control. However, no apparent increase in superoxide levels was observed in cells harboring c.863T>G (103.2%) or c.1505T>A (102.5%).

3.3 Cells containing mutant VLCAD prone to apoptosis without glucose

To directly assess cell fate due to VLCAD defects under physiological stress, cell apoptosis was measured in the presence or absence of glucose (Fig. 3). No marked changes of apoptotic cell populations were observed in cell lines cultured under normal conditions. After 12 h starvation without glucose, however, the population of apoptotic cells in variants c.541C>T, c.863T>G, c.895A>G, c.1153C>T, c.1238T>C, c.1276G>A, and c.1505T>A increased dramatically, by 3.10, 2.65, 2.45, 3.45, 2.00, 5.60, and 4.25 times, respectively, compared to apoptotic cell numbers in control cells. These results indicate that apoptosis in VLCAD-deficient cells increased under glucose limitation, which concurs with the results of previous experiments on fibroblasts with VLCAD deficiencies (Seminotti et al., 2019).

3.4 Influences of variants on the stability of VLCAD dimer and its MD simulation

VLCAD usually forms functional homodimers. In order to investigate whether the VLCAD variants have potentially deleterious effects on the stability of the VLCAD dimer, a total of 10 μg protein from each cell line expressing mutant and WT HA-tagged VLCAD was separated by BN-PAGE and then hybridized with anti-HA. As shown in Fig. 4a, dimer stabilities in most variants were notably disturbed compared to those of control cells. The ratios of dimer per total protein in c.541C>T, c.863T>G, c.895A>G, c.1153C>T, c.1238T>C, c.1276G>A, and c.1505T>A were 80.1%, 72.5%, 78.4%, 22.7%, 36.7%, 166.4%, and 89.0% of those in control cells, respectively. All of the novel six variants in different domains displayed diverse changes in VLCAD stability. As the

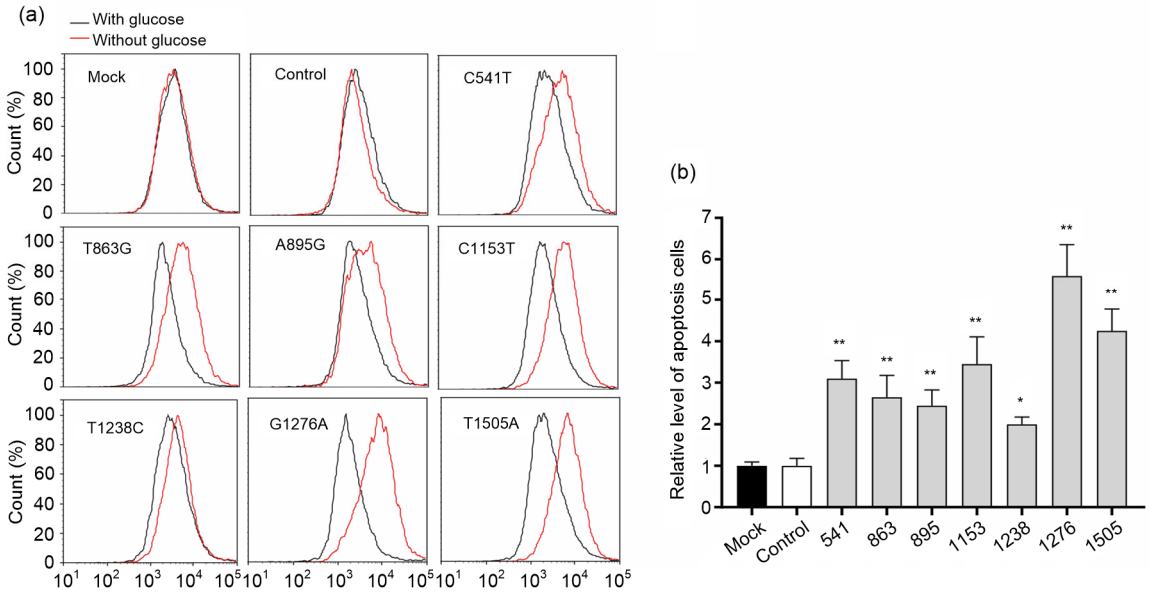

Fig. 3 Analysis of apoptosis in cell lines

(a) Apoptosis levels in untreated HEK293T, control, and mutant cell lines with (black) or without (red) glucose. The proportions of apoptotic cells in mutant cell lines (c.541C>T, c.863T>G, c.895A>G, c.1153C>T, c.1238T>C, c.1276G>A, and c.1505T>A) without glucose were (20.3±2.8)%, (17.8±3.9)%, (16.3±2.8)%, (23.0±4.7)%, (13.3±0.8)%, (37.3±4.8)%, and (28.7±3.5)%, respectively. (b) Changes in the proportion of apoptotic cells without glucose. Data were normalized to the mean value of control. Data were expressed as mean±standard deviation (SD), n=3. * P≤0.05, ** P≤0.01, vs. control. Samples were described as in Fig. 1

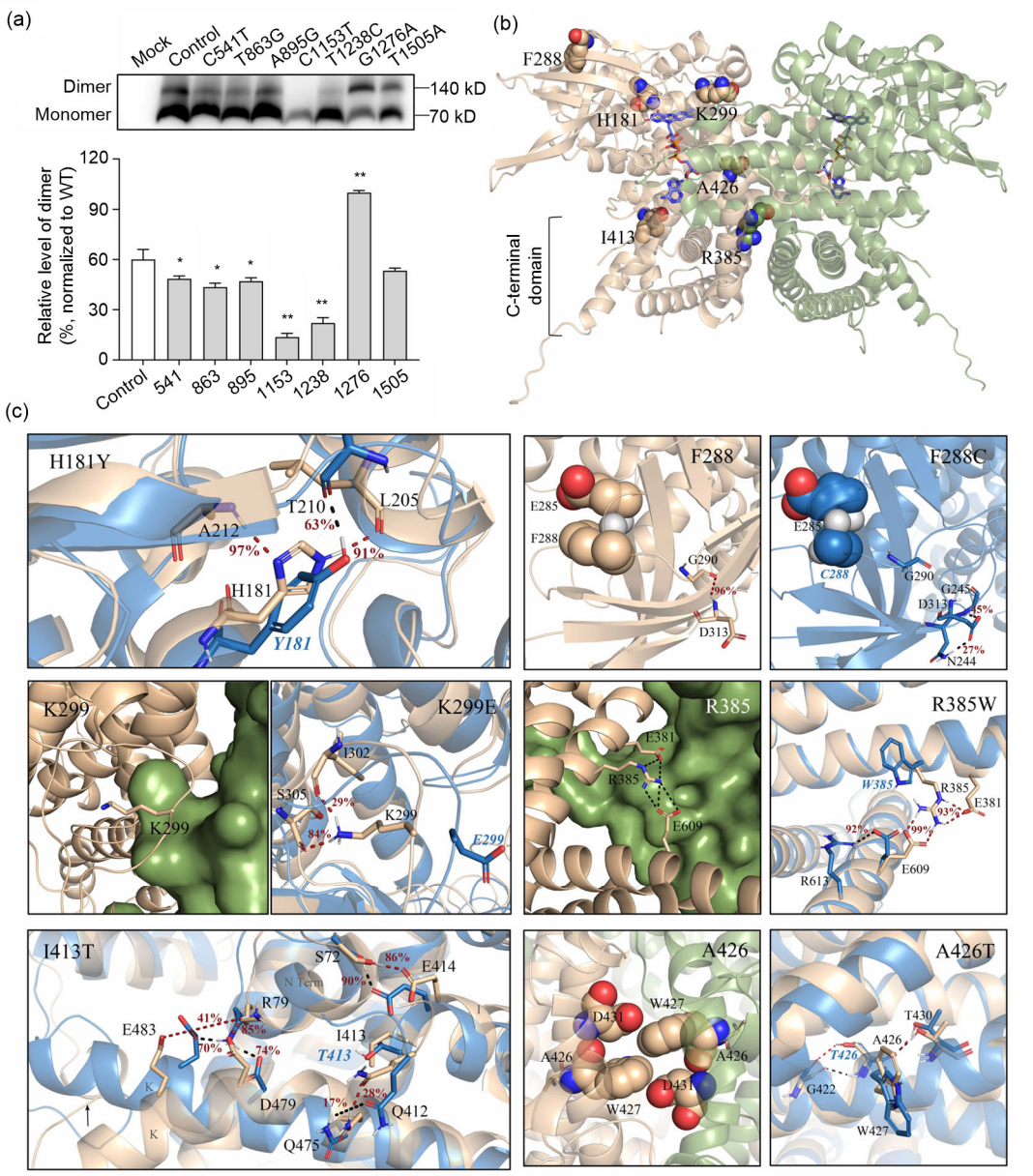

Fig. 4 Stability and molecular dynamics simulation analyses of VLCAD

(a) Stability of very-long-chain acyl-CoA dehydrogenase (VLCAD) in blue native-polyarylamide gel electrophoresis (BN-PAGE). The relative levels of mutant VLCAD dimer per total protein were normalized to the mean value of the control. Samples were described as in Fig. 1. Data were expressed as mean±standard deviation (SD), n=3. * $P\leq0.05$, ** $P\leq0.01$, vs. control. (b) Location of the six variants on the dimeric structure of wild-type (WT) VLCAD (PDB ID: 2UXW) with its cofactor, flavin adenine dinucleotide (FAD). Each WT monomer is represented in tan or green. (c) Structural predictions in WT and mutant residues. The structure of the mutant is shown in sky-blue with the WT in tan or green. The black and red dashed lines represent the electrostatic interactions of mutant and WT residues, respectively. The occupancy of the hydrogen bonds is shown in red

stability of dimer may be due to the position of residues within the protein structure, we analyzed the location of residues according to the existing structure model of the homodimer (Fig. 4b). Residues H181, F288, and K299 lay in the catalytic domain of each monomer. The residue K299 occurred near the site that the flavin adenine dinucleotide (FAD) cofactor binding to, and predicted to stabilize the FAD cofactor (McAndrew et al., 2008). Residues R385, I413, A426, and L502 localized in the C-terminal domain,

which is thought to bind to the inner mitochondrial membrane (McAndrew et al., 2008). However, residues R385, I413, and A426 most likely contributed to the stability of dimer, since they were localized in the contact surfaces of two monomers within the dimer.

To determine whether the variants may affect the stability of VLCAD, MD simulations of six residues (except p.L502Q) were analyzed with GROMACS 4.5.5 packages (Fig. 4c) (A larger version of Fig. 4c is available in Fig. S4). In our prediction model, the imidazole group of WT His181 interacted with helix residue Ala212 and β-strand residue Leu205 by a hydrogen bond, whereas variant Tyr181 introduced new electrostatic interactions with residue Thr210 in the loop region. When Phe288 was changed to Cys288, a large conformational change of the β-sheet, which normally formed on the edge of the aromatic ring of Phe288 with the negatively charged residue Glu285 (Philip et al., 2011), was destroyed by the interaction between D313 and G245 or N244. When the basic residue lysine was changed to glutamic acid, E299 faced outward of the electrostatic interactions loop initially formed by K299 with adjacent S305 and I302. In simulations of R385W, the inter-helical salt bridge at R385–E609 (with an occupancy of 99%) was replaced with a new intra-helical interaction between R613 and E609. When the non-polar amino acid isoleucine (I) was changed to the polar amino acid threonine (T), T413 strengthened the R79–E483 salt bridge located on N-terminal and helix K from 41% occupancy to 70%, leading to lower flexibility of helix K and helical bending for inner membrane binding. In the case of A426T, binding to the backbone nitrogen atom of G422 was changed from the carbonyl oxygen atom of A426 to the side-chain hydroxy oxygen atom, which in turn switched the χ^{-2} dihedral angle (CA-CB-CG-CD1) of W427 from gauche (−) to the gauche (+) conformation, resulting in a shifted orientation of W427.

4 Discussion

VLCAD deficiencies vary greatly in terms of clinical phenotypes and genetic variants. In this study, we demonstrated that all of the six novel variants in VLCAD deficiency directly impaired enzyme activity for FAO. Cells carrying these variants exhibited a marked FAO deficiency in oxidizing palmitate as reported in earlier work (Schiff et al., 2013; Merritt et al., 2018). Besides the reported pathogenic variant c.1153C>T, undetectable FAO activity was found in cells carrying c.863T>G, c.895A>G, c.1238T>C, c.1276G>A, and c.1505T>A, while c.541C>T cells showed a decreased capacity to utilize FAs. Moreover, the perturbation of FAO led to defects in mitochondrial function, including decreases in mitochondrial respiratory-chain function and ATP generation, accompanied by increased levels of ROS. However, the mitochondrial defects found in each variant also had specific characteristics. For instance, cells harboring c.541C>T had only a minor decrease in mitochondrial ATP production since c.541C>T retained a certain capacity to utilize exogenous palmitate for ATP generation. The lowest basal oxygen consumption in FAO was observed in cells carrying c.895A>G. Though long-chain acyl-CoA dehydrogenase has been reported as a source of mitochondrial hydrogen peroxide (Zhang et al., 2019), no significant elevation of superoxide was observed in c.863T>G or c.1505T>A under stress, while ROS increased notably in cells carrying c.1276G>A even without H_2O_2 stimulation. For this reason, we speculate that patients harboring c.1276G>A might respond to some extent to ROS scavengers, as suggested elsewhere (Seminotti et al., 2019). Intriguingly, higher apoptosis levels were found in cells carrying mutant VLCAD under glucose-limited stress, especially in cells carrying c.1276G>A or c.1505T>A mutations. The finding of increased levels of apoptosis under glucose-limited stress provides some biochemical evidence for prevention of catabolic fasting stress as a key rationale for dietary treatment for VLCAD deficiency (Gillingham et al., 2006). It was also likely explaining the fact that some patients carrying VLCAD variants were “asymptomatic” under conditions without metabolic stress, but developed muscle weakness associated with exercise due to the inability to maintain adequate caloric intake (Behrend et al., 2012).

The specific effects of variants on mitochondrial function may be associated primarily with the residue position of these variants in VLCAD protein structure. The mature VLCAD is a homodimer associated with the mitochondrial inner membrane (Souri et al., 1998; McAndrew et al., 2008). Thus, variants should have different effects on the stability or activity of the protein. Changes in VLCAD stability influences the physical interaction of VLCAD with trifunctional

protein (TFP), leading to impaired ATP production (Wang et al., 2019). In fact, we found that all six novel variants disturbed the stability of VLCAD. The ratios of dimer in the amount of VLCAD protein were markedly reduced in c.541C>T, c.863T>G, c.895A>G, c.1238T>C, and c.1505T>A, but increased notably in c.1276G>A, related to the WT control. Additionally, molecular dynamics analysis predicts that all variants other than c.1505T>A should have major conformational changes. Based on what is known about the molecular structure of VLCAD, the siting of residues H181Y (c.541C>T), F288C (c.863T>G), and K299E (c.895A>G) in the catalytic domain of VLCAD suggests that these variants may primarily have effects on the catalytic activity of this enzyme in FAO. Cells with K299E exhibited the lowest basal OCRs, with a mild decrease in both protein expression and homodimer stability, which is consistent with the conclusion that the K299 is a key site affecting FAD binding for enzyme activity (McAndrew et al., 2008). As VLCAD uses enzyme-bound FAD as the electron acceptor, riboflavin supplementation might improve its activity in patients carrying K299E (Schiff et al., 2013; Bleeker et al., 2019). The other three residues, I413T (c.1238T>C), A426T (c.1276G>A), and L502Q (c.1505T>A), are located in the C-terminal domain. The cells harboring c.1238T>C had the lowest VLCAD dimer stability, whereas the c.1276G>A variant tended to strengthen dimer stability compared to that of the WT VLCAD. The data suggest that these two alterations may be critical for VLCAD stability, and ultimately result in mitochondrial dysfunction (Seminotti et al., 2019). In contrast, no obvious decrease in the homodimer was observed in cells carrying c.1505T>A, which is in agreement with previous predictions that this residue may play a role in anchoring VLCAD to the inner mitochondrial membrane (McAndrew et al., 2008). Moreover, the hypothesis of functional consequences due to genetic mutations in all six variants was further supported by predictions of a broken original thermodynamic structure by MD simulation in all six variants.

5 Conclusions

Collectively, the six pathogenic variants found in patients with mild symptoms impaired the FAO capacity and resulted in mitochondrial dysfunction in various ways. The combined biochemical analysis and structural predictions of each variant provide important clues to the molecular basis of pathogenesis in each VLCAD mutant. These data on VLCAD-deficient phenotypes will be helpful in future management of diagnosis and treatment for VLCAD deficiencies.

Contributors

Ping-ping JIANG and Qiang SHU designed the research, wrote the manuscript, and had primary responsibility for final content. Ting CHEN and Fan TONG conducted the biochemical experiments and drafted the manuscript. Xiao-yu WU performed the cell culture and mitochondrial function analysis. Ling ZHU and Jing ZHENG supported the interpretation of the molecular genetics data. Ting CHEN, Xiao-hui CANG, and Qiu-zi YI were responsible for molecular dynamics analysis. Fan TONG, Ru-lai YANG, and Zheng-yan ZHAO carried out the clinical evaluation.

Acknowledgments

We thank all patients and their family members for their participation.

Compliance with ethics guidelines

Ting CHEN, Fan TONG, Xiao-yu WU, Ling ZHU, Qiu-zi YI, Jing ZHENG, Ru-lai YANG, Zheng-yan ZHAO, Xiao-hui CANG, Qiang SHU, and Ping-ping JIANG declare that they have no conflicts of interest.

All procedures followed were in accordance with the ethical standards of the responsible committee on human experimentation (institutional and national) and with the Helsinki Declaration of 1975, as revised in 2008 (5). Informed consent was obtained from all patients for being included in the study.

References

Andresen BS, Olpin S, Poorthuis BJHM, et al., 1999. Clear correlation of genotype with disease phenotype in very-long-chain acyl-CoA dehydrogenase deficiency. *Am J Hum Genet*, 64(2):479-494. https://doi.org/10.1086/302261

Aoyama T, Souri M, Ushikubo S, et al., 1995. Purification of human very-long-chain acyl-coenzyme A dehydrogenase and characterization of its deficiency in seven patients. *J Clin Invest*, 95(6):2465-2473. https://doi.org/10.1172/JCI117947

Behrend AM, Harding CO, Shoemaker JD, et al., 2012. Substrate oxidation and cardiac performance during exercise in disorders of long chain fatty acid oxidation. *Mol Genet Metab*, 105(1):110-115. https://doi.org/10.1016/j.ymgme.2011.09.030

Berendsen HJC, Postma JPM, van Gunsteren WF, et al., 1984. Molecular dynamics with coupling to an external bath. *J*

Chem Phys, 81(8):3684-3690. https://doi.org/10.1063/1.448118

Bleeker JC, Kok IL, Ferdinandusse S, et al., 2019. Proposal for an individualized dietary strategy in patients with very long-chain acyl-CoA dehydrogenase deficiency. *J Inherit Metab Dis*, 42(1):159-168. https://doi.org/10.1002/jimd.12037

Boneh A, Andresen BS, Gregersen N, et al., 2006. VLCAD deficiency: pitfalls in newborn screening and confirmation of diagnosis by mutation analysis. *Mol Genet Metab*, 88(2):166-170. https://doi.org/10.1016/j.ymgme.2005.12.012

Bramucci E, Paiardini A, Bossa F, et al., 2012. PyMod: sequence similarity searches, multiple sequence-structure alignments, and homology modeling within PyMOL. *BMC Bioinformatics*, 13:S2. https://doi.org/10.1186/1471-2105-13-S4-S2

Buck MD, O'Sullivan D, Klein Geltink RI, et al., 2016. Mitochondrial dynamics controls T cell fate through metabolic programming. *Cell*, 166(1):63-76. https://doi.org/10.1016/j.cell.2016.05.035

Cecatto C, Amaral AU, da Silva JC, et al., 2018. Metabolite accumulation in VLCAD deficiency markedly disrupts mitochondrial bioenergetics and Ca^{2+} homeostasis in the heart. *FEBS J*, 285(8):1437-1455. https://doi.org/10.1111/febs.14419

Essmann U, Perera L, Berkowitz ML, et al., 1995. A smooth particle mesh Ewald method. *J Chem Phys*, 103(19): 8577-8593. https://doi.org/10.1063/1.470117

Gillingham MB, Scott B, Elliott D, et al., 2006. Metabolic control during exercise with and without medium-chain triglycerides (MCT) in children with long-chain 3-hydroxy acyl-CoA dehydrogenase (LCHAD) or trifunctional protein (TFP) deficiency. *Mol Genet Metab*, 89(1-2): 58-63. https://doi.org/10.1016/j.ymgme.2006.06.004

Hess B, 2008. P-LINCS: a parallel linear constraint solver for molecular simulation. *J Chem Theory Comput*, 4(1):116-122. https://doi.org/10.1021/ct700200b

Hess B, Kutzner C, van der Spoel D, et al., 2008. GROMACS 4: algorithms for highly efficient, load-balanced, and scalable molecular simulation. *J Chem Theory Comput*, 4(3):435-447. https://doi.org/10.1021/ct700301q

Huang J, Mackerell AD Jr, 2013. CHARMM36 all-atom additive protein force field: validation based on comparison to NMR data. *J Comput Chem*, 34(25):2135-2145. https://doi.org/10.1002/jcc.23354

Humphrey W, Dalke A, Schulten K, 1996. VMD: visual molecular dynamics. *J Mol Graph*, 14(1):33-38. https://doi.org/10.1016/0263-7855(96)00018-5

Jiang PP, Wang M, Xue L, et al., 2016. A hypertension-associated $tRNA^{Ala}$ mutation alters tRNA metabolism and mitochondrial function. *Mol Cell Biol*, 36(14):1920-1930. https://doi.org/10.1128/MCB.00199-16

Li XY, Ding Y, Ma YY, et al., 2015. Very long-chain acyl-coenzyme A dehydrogenase deficiency in Chinese patients: eight case reports, including one case of prenatal diagnosis. *Eur J Med Genet*, 58(3):134-139. https://doi.org/10.1016/j.ejmg.2015.01.005

Lim SC, Tajika M, Shimura M, et al., 2018. Loss of the mitochondrial fatty acid β-oxidation protein medium-chain acyl-coenzyme A dehydrogenase disrupts oxidative phosphorylation protein complex stability and function. *Sci Rep*, 8:153. https://doi.org/10.1038/s41598-017-18530-4

McAndrew RP, Wang YD, Mohsen AW, et al., 2008. Structural basis for substrate fatty acyl chain specificity: crystal structure of human very-long-chain acyl-CoA dehydrogenase. *J Biol Chem*, 283(14):9435-9443. https://doi.org/10.1074/jbc.M709135200

Merritt JL II, Norris M, Kanungo S, 2018. Fatty acid oxidation disorders. *Ann Transl Med*, 6(24):473. https://doi.org/10.21037/atm.2018.10.57

Miller MJ, Burrage LC, Gibson JB, et al., 2015. Recurrent *ACADVL* molecular findings in individuals with a positive newborn screen for very long chain acyl-coA dehydrogenase (VLCAD) deficiency in the United States. *Mol Genet Metab*, 116(3):139-145. https://doi.org/10.1016/j.ymgme.2015.08.011

Nomura M, Liu J, Rovira II, et al., 2016. Fatty acid oxidation in macrophage polarization. *Nat Immunol*, 17(3):216-217. https://doi.org/10.1038/ni.3366

Obaid A, Nashabat M, Alfadhel M, et al., 2018. Clinical, biochemical, and molecular features in 37 Saudi patients with very long chain acyl CoA dehydrogenase deficiency. *In*: Morava E, Baumgartner M, Patterson M, et al. (Eds.), JIMD Reports, Volume 40. Springer, Berlin, p.47-53. https://doi.org/10.1007/8904_2017_58

Pena LDM, van Calcar SC, Hansen J, et al., 2016. Outcomes and genotype-phenotype correlations in 52 individuals with VLCAD deficiency diagnosed by NBS and enrolled in the IBEM-IS database. *Mol Genet Metab*, 118(4):272-281. https://doi.org/10.1016/j.ymgme.2016.05.007

Philip V, Harris J, Adams R, et al., 2011. A survey of aspartate-phenylalanine and glutamate-phenylalanine interactions in the protein data bank: searching for anion-π pairs. *Biochemistry*, 50(14):2939-2950. https://doi.org/10.1021/bi200066k

Schiff M, Mohsen AW, Karunanidhi A, et al., 2013. Molecular and cellular pathology of very-long-chain acyl-CoA dehydrogenase deficiency. *Mol Genet Metab*, 109(1):21-27. https://doi.org/10.1016/j.ymgme.2013.02.002

Seminotti B, Leipnitz G, Karunanidhi A, et al., 2019. Mitochondrial energetics is impaired in very long-chain acyl-CoA dehydrogenase deficiency and can be rescued by treatment with mitochondria-targeted electron scavengers. *Human Mol Genet*, 28(6):928-941. https://doi.org/10.1093/hmg/ddy403

Souri M, Aoyama T, Hoganson G, et al., 1998. Very-long-chain acyl-CoA dehydrogenase subunit assembles to the dimer form on mitochondrial inner membrane. *FEBS Lett*, 426(2):187-190. https://doi.org/10.1016/s0014-5793(98)00343-3

Tong F, Chen T, Jiang PP, et al., 2019. Analysis of *ACADVL* gene variations among nine neonates with very long chain acyl-CoA dehydrogenase deficiency. *Chin J Med Genet*, 36(4):310-313 (in Chinese). https://doi.org/10.3760/cma.j.issn.1003-9406.2019.04.005

Wajner M, Amaral AU, 2015. Mitochondrial dysfunction in fatty acid oxidation disorders: insights from human and animal studies. *Biosci Rep*, 36(1):e00281. https://doi.org/10.1042/BSR20150240

Wang YD, Palmfeldt J, Gregersen N, et al., 2019. Mitochondrial fatty acid oxidation and the electron transport chain comprise a multifunctional mitochondrial protein complex. *J Biol Chem*, 294(33):12380-12391. https://doi.org/10.1074/jbc.RA119.008680

Wittig I, Braun HP, Schägger H, 2006. Blue native page. *Nat Protoc*, 1(1):418-428. https://doi.org/10.1038/nprot.2006.62

Xiong JH, 2018. Fatty acid oxidation in cell fate determination. *Trends Biochem Sci*, 43(11):854-857. https://doi.org/10.1016/j.tibs.2018.04.006

Yang JY, Yan RX, Roy A, et al., 2015. The I-TASSER suite: protein structure and function prediction. *Nat Methods*, 12(1):7-8. https://doi.org/10.1038/nmeth.3213

Yu JL, Xiao Y, Liu JX, et al., 2014. Loss of MED1 triggers mitochondrial biogenesis in C2C12 cells. *Mitochondrion*, 14:18-25. https://doi.org/10.1016/j.mito.2013.12.004

Zhang DY, Liu ZX, Choi CS, et al., 2007. Mitochondrial dysfunction due to long-chain acyl-CoA dehydrogenase deficiency causes hepatic Steatosis and hepatic insulin resistance. *Proc Natl Acad Sci USA*, 104(43):17075-17080. https://doi.org/10.1073/pnas.0707060104

Zhang RN, Li YF, Qiu WJ, et al., 2014. Clinical features and mutations in seven Chinese patients with very long chain acyl-CoA dehydrogenase deficiency. *World J Pediatr*, 10(2):119-125. https://doi.org/10.1007/s12519-014-0480-2

Zhang YX, Bharathi SS, Beck ME, et al., 2019. The fatty acid oxidation enzyme long-chain acyl-CoA dehydrogenase can be a source of mitochondrial hydrogen peroxide. *Redox Biol*, 26:101253. https://doi.org/10.1016/j.redox.2019.101253

Zhao XX, Han JM, Zhu L, et al., 2018. Overexpression of human mitochondrial alanyl-tRNA synthetase suppresses biochemical defects of the mt-tRNA^{Ala} mutation in cybrids. *Int J Biol Sci*, 14(11):1437-1444. https://doi.org/10.7150/ijbs.27043

List of electronic supplementary materials

Fig. S1 Variants in VLCAD-deficient patients and their conservation of residues

Fig. S2 Expression levels of HA-tagged VLCAD in cells

Fig. S3 FAO capacity for utilization of exogenous palmitate

Fig. S4 Structural predictions in wild-type and mutant residues

中文概要

题　目：极长链酰基辅酶 A 脱氢酶缺乏症 *ACADVL* 基因新发突变导致线粒体功能障碍

目　的：鉴定并阐述 6 个 *ACADVL* 新发突变的对细胞和分子功能的影响，为后期分子诊断和临床病例管理提供科学依据。

创新点：本文从分子功能和结构的角度阐述 6 个新位点对蛋白和细胞功能的不同影响。

方　法：通过体外构建突变载体建立各突变的过表达细胞系，检测各细胞系脂肪酸代谢能力、线粒体呼吸链功能、线粒体产三磷酸腺苷（ATP）能力、活性氧（ROS）和凋亡水平。同时检测了新发突变对蛋白二聚体稳定性的影响并用分子动力学模拟了突变蛋白构像的改变。

结　论：突变（c.541C>T、c.863T>G、c.895A>G、c.1238T>C、c.1276G>A 和 c.1505T>A）过表达细胞系均表现出脂肪酸代谢障碍，线粒体呼吸链功能障碍，ATP 产生水平下降和线粒体 ROS 水平上升。在无糖条件下，各细胞系的凋亡水平上升。各突变影响了极长链酰基辅酶 A 脱氢酶（VLCAD）蛋白二聚体的稳定性，分子动力学模拟预测每个突变均会导致 VLCAD 蛋白结构的发生重要构象变化。

关键词：线粒体功能障碍；极长链酰基辅酶 A 脱氢酶缺乏症；β 氧化；分子动力学模拟